Heavy rainfall in Mediterranean cyclones. Part I: contribution of deep convection and warm conveyor belt

Article

Accepted Version

www.reading.ac.uk/centaur

Heavy rainfall in Mediterranean cyclones, Part I: Contribution of deep convection and warm conveyor belt

Emmanouil Flaounas[1], Vassiliki Kotroni[1], Konstantinos Lagouvardos[1], Suzanne Gray[2], Jean-François Rysman[3], Chantal Claud[3]

1) National Observatory of Athens, Greece
2) Department of Meteorology, University of Reading, UK
3) Laboratoire de Métérology Dynamique, Institut Pierre Simon Laplace CNRS, École Polytechnique, Université Paris-Saclay, Palaiseau, France

Abstract
In this study, we provide an insight to the role of deep convection (DC) and the warm conveyor belt (WCB) as leading processes to Mediterranean cyclones' heavy rainfall. To this end, we use reanalysis data, lighting and satellite observations to quantify the relative contribution of DC and the WCB to cyclone rainfall, as well as to analyse the spatial and temporal variability of these processes with respect to the cyclone centre and life cycle.

Results for the period 2005-2015 show that the relationship between cyclone rainfall and intensity has high variability and demonstrate that even intense cyclones may produce low rainfall amounts. However, when considering rainfall averages for cyclone intensity bins, a linear relationship was found. We focus on the 500 most intense tracked cyclones (responsible for about 40-50% of the total 11-year Mediterranean rainfall) and distinguish between the ones producing high and low rainfall amounts. DC and the WCB are found to be the main cause of rainfall for the former (producing up to 70% of cyclone rainfall), while, for the latter, DC and the WCB play a secondary role (producing up to 50% of rainfall). Further analysis showed that rainfall due to DC tends to occur close to the cyclones' centre and to their eastern sides, while the WCBs tend to produce rainfall towards the northeast. In fact, about 30% of rainfall produced by DC overlaps with rainfall produced by WCBs but this represents only about 8% of rainfall produced by WCBs. This suggests that a considerable percentage of DC is associated with embedded convection in WCBs. Finally, DC was found to be able to produce higher rain rates than WCBs, exceeding 50 mm in 3-hourly accumulated rainfall compared to a maximum of the order of 40 mm for WCBs.

Our results demonstrate in a climatological framework the relationship between cyclone intensity and processes that lead to heavy rainfall, one of the most prominent environmental risks in the Mediterranean. Therefore, we set perspectives for a deeper analysis of the favourable atmospheric conditions that yield high impact weather.

1. Introduction
Mediterranean cyclones are associated with upper-tropospheric precursors, such as wave breaking, cut-offs and troughs, and typically tend to develop within a baroclinic environment (Fita et al. 2006; Campins et al. 2006; Homar et al. 2007; Grams et al. 2011; Flaounas et al. 2015). In fact, Mediterranean cyclones may be considered as a distinct class of extra-tropical cyclones. In contrast to other cyclones that develop over oceans, they form within a relatively small region, surrounded by high mountains, where even the most intense systems are expected to have comparably smaller size, weaker intensity and shorter lifetime (Trigo, 2006; Čampa and Wernli, 2012). Despite being considered as relatively weak systems, Mediterranean cyclones figure among the most prominent environmental risks of the region (Llasat-Botija et al. 2007). Related risks are associated with heavy rainfall, wind storms, hailstorms, wind surges etc. Such events are found in the vicinity of the cyclones' centres affecting several areas within their passage (Jansa et al. 2001; Nissen et al. 2010; Raveh-Rubin and Wernli, 2015).

In this study, we focus on Mediterranean cyclones that produce heavy rainfall. Several previous case studies have highlighted the relationship between Mediterranean cyclones and high impact weather: associated rainfall has been reported to exceed 100 mm (e.g. Lagouvardos et al. 1996; Kotroni et al. 1999; Romero, 2001; Lionello et al. 2006; Lagouvardos et al. 2007a; Davolio et al. 2009; Miglietta et al. 2013). In a climatological framework, few studies have been devoted to quantifying the contribution of Mediterranean cyclones to the total regional

rainfall. Nevertheless, estimations show an average contribution that may exceed 70%, especially in winter (Hawcroft et al. 2012; Pfahl and Wernli 2012; Flaounas et al. 2016a). In particular for heavy rainfall and extremes, Jansa et al. (2001) used ground observations along the west Mediterranean coasts to show that more than 90% of cases of daily rainfall exceeding 60 mm are related to cyclones. More recently, Pfahl et al. (2014) and Flaounas et al. (2016a) analysed climatological datasets from reanalysis data and models and found that about 60 to 95% of rainfall extremes, depending on the area, are related to Mediterranean cyclones.

In several studies, deep convection (DC) and the warm conveyor belt (WCB) have been highlighted as the main mechanisms for producing heavy rainfall in cyclonic systems (Claud et al. 2010, 2012; Pfahl et al. 2014; Flaounas et al. 2016b). DC refers to strong updraughts of air masses within clouds, while the WCB refers to fast ascending air masses that rise slantwise over the extra-tropical cyclone's warm front. The relative contribution of these processes to cyclone-produced rainfall in the Mediterranean is, however, still unclear. Claud et al. (2012) used diagnostics based on satellite observations to show that the areas of frequent DC overlap with the regions of high cyclone track density. Their DC diagnostics were associated with rain rates of more than 20 mm per 3 hours (Funatsu et al. 2007), suggesting that DC significantly contributes to heavy rainfall in Mediterranean cyclones. The important role of DC in producing heavy rainfall in cyclones has also been highlighted in several case studies (e.g. Lagouvardos and Kotroni, 2007; Claud et al.,et al. 2010; McTaggart-Cowan, 2010; Miglietta et al. 2013). Concerning WCBs, Ziv et al. (2010) and Flaounas et al. (2015) analysed Mediterranean cyclones WCBs and discussed that these WCBs are typically poorer in water content than the ones that rise over oceans. This is due to the relatively small surface area of the Mediterranean Sea which limits the ability of air masses to draw water by evaporation before their ascent. Nevertheless, Pfahl et al. (2014) used reanalysis data to show that WCBs are responsible for about half of the total Mediterranean rainfall extremes.

Both DC and the WCB may significantly contribute to cyclone heavy rainfall, while it is not uncommon that DC is embedded in WCBs. For instance, Martínez-Alvarado et al. (2014) analysed the dichotomous cyclonic and anticyclonic branches of the WCB of a cyclone case that occurred over the North Atlantic. In their analysis, only the anticyclonic branch was associated with embedded convection. More recently, Rasp et al. (2016) showed in two case studies that the ascent of air masses in WCBs could be either associated with embedded convection or with "non-convective" slantwise ascent. Flaounas et al. (2016b) recently analysed two deep cyclones that developed in the western Mediterranean. Both cyclones presented similar sea level pressure at their centre (about 985 hPa) and similar rainfall accumulations in the western Mediterranean (ground stations measured a maximum rainfall accumulation of approximately 180 mm due to each cyclone). The use of airborne radar observations and operational analysis showed that DC was present only in one of the two cyclones (alongside a WCB), while, in the other cyclone, almost all heavy rainfall was due to its WCB. Consequently, two intense cyclones that had similar area, pressure depth and time period of occurrence had different dynamical and thermodynamical mechanisms for producing heavy rainfall. In fact, DC and WCBs in Mediterranean cyclones may present a high variability from case to case. Raveh-Rubin and Wernli (2016) analysed five high-impact Mediterranean cyclones and showed that all of them produced rainfall due to WCBs. However, convective rainfall was produced in the core of four cyclones and at the cold front of two. In a climatological framework, Galanaki et al. (2016) used lightning observations to address the issue of DC in cyclone cores. Their results suggest that about one third of intense cyclones may develop DC close to their centre, while, in the other two thirds, no lightning was observed at all. The frequency of occurrence and the contribution of DC and WCBs to rainfall in Mediterranean cyclones is thus still an open question.

To better understand high-impact weather in Mediterranean cyclones and especially their capacity to produce heavy rainfall, we need to gain deeper insight into the relevant cyclone processes. In this article, we analyse DC and the WCB as leading processes for producing heavy rainfall in Mediterranean cyclones. The application of a novel approach permits the quantification of the relationship between cyclones intensity, rainfall, DC and WCB in a climatological framework, enabling us to address the following questions:

1) How are the intensity and rainfall of Mediterranean cyclones related?

2) What is the relative contribution of DC and the WCB to rainfall in these cyclones?

108   3) What is the spatial and temporal variability of DC and the WCB relative to cyclone centres and life cycles?

The rest of the paper is organised as follows: the next section describes in detail the datasets we used, as well as
111   our methodological approach. Results are presented in sections 3 and 4, while section 5 contains our concluding remarks.

114   **2. Datasets and Methodology**

2.1 Reanalysis, cyclone tracking and observations
117   All atmospheric fields in this study have been extracted from the ERA-Interim (ERAI) reanalysis of the European Centre for Medium-Range Weather Forecasts (ECMWF; Dee et al. 2011), available every 6 hours (at 0000, 0600, 1200 and 1800 UTC) and interpolated to a standard 0.25°x0.25° grid in longitude and latitude.
120

Mediterranean cyclones have been tracked for the 11-year period of 2005-2015, applying the method of Flaounas et al. (2014) to the fields of relative vorticity at the atmospheric pressure level of 850 hPa. Cyclone track-
123   ing has been performed in two steps. First, relative vorticity has been smoothed in each 6-hourly time step of ERAI by applying three times a spatial moving average of 1.25 deg² (i.e., fields have been smoothed using a spatial window of 5×5 grid points). Cyclone centres were identified as local maxima of relative vorticity of at least
126   3×10^{-5} s^{-1}. Second, tracks have been defined by connecting cyclone centres in consecutive time steps. To define tracks, the tracking algorithm starts from the most intense cyclone identified (i.e. the one with maximum relative vorticity) and searches backward and forward in time for all of its possible tracks. Cyclone centres are connected
129   in consecutive time steps if they are located within an area of 5°x3° in longitude and latitude. Of all possible cyclone tracks, the algorithm retains the one that presents the least average difference in relative vorticity between consecutive track points, weighted by the distance between the track points. This method has been recently as-
132   sessed, along with five other methods, in Flaounas et al. (2017) using both ERAI and regional climate models. Compared to the other methods, the method of Flaounas et al, (2014) does not use strict criteria to define cyclones and thus a large number of weak cyclone tracks may be identified. However, when comparing the Fla-
135   ounas et al. (2014) results to those from the other methods in the reproduction of the climatology of intense Mediterranean cyclones, the method by Flaounas et al. (2014) provides realistic results consistently capturing the cyclones' seasonal cycle and their spatial variability of occurrence. Further assessment of the tracking method of
138   Flaounas et al. (2014) along with other methods may be also found in Rudeva et al. (2014), Lionello et al. (2016) and Pinto et al. (2016).

141   In this study we retained only cyclones that last at least 24 hours (i.e. that have at least five track points) and have their mature stage located within 5°W to 40°E and 30°N to 46°N, excluding cyclone tracks occurring over the Atlantic Ocean (i.e. all cyclones occurring west of 2.5°E and north of 43°N) and over the Black Sea (i.e. all
144   cyclones occurring east of 27°E and north of 41°N). These criteria resulted in a cyclone climatology composed of 7091 cyclones. Figure 1 shows the Mediterranean region topography and the area where cyclone tracking has been applied.
147

To associate cyclones with rainfall, we used estimates provided by the Tropical Rainfall Measuring Mission (TRMM) 3B42 algorithm. In addition to TRMM data, this algorithm takes into account observations from other
150   satellite platforms and provides estimations of rainfall accumulations in 3-hourly time steps (at 0000, 0300, 0600, 0900, 1200, 1500, 1800 and 2100 UTC). The estimations are available on a regular grid of 0.25°x0.25° in longitude and latitude (Huffman et al. 2007; Romilly and Gebremichael, 2011). Rainfall rates are representative
153   of a time range of +/- 1.5 hours, centred on the 3-hourly time steps.

Lightning data were provided by the very low frequency lightning detection network ZEUS, operated by the Na-
156   tional Observatory of Athens (Kotroni and Lagouvardos, 2008, 2016). ZEUS provides real-time data since 2005 (www.thunderstorm24.com).

159   Passive microwave radiometers are able to detect atmospheric cloud ice due to the strong scattering of radiation

by ice crystals, especially at frequencies around the water vapour absorption line (183.3 GHz). Instruments that probe around the water vapour absorption line tend to be mainly sensitive to ice in the mid to high troposphere. Since heavy loading of ice in the mid to high troposphere is a characteristic signature of convective activity, Hong et al. (2005) developed a diagnostic to detect DC using AMSU-B (Advanced Microwave Sounding Unit-B) measurements frequencies: the diagnostic has since been assessed in the Mediterranean by Funatsu et al. (2007) and Rysman et al. (2015). To get the most comprehensive overview of deep convection in the Mediterranean, we used passive microwave radiometers available during the 2005-2015 period. Observations have been taken from the AMSU-B instruments on-board the National Oceanic and Atmospheric Administration (NOAA) satellites 15-17, the Microwave Humidity Sounder (MHS) on-board the European Operational Meteorological satellite A & B, the Special Sensor Microwave Imager/Sounder (SSMIS) on-board the Defense Meteorological Satellite Program – F16-18 and the Advanced Technology Microwave Sounder (ATMS) on-board the Suomi National Polar-orbiting Partnership. All these instruments probe around the water absorption line with frequencies very similar to AMSU-B. Each DC event detected by the passive microwave sounders has been summed up on a 0.2°x0.2° grid every 3 hours.

Finally, cyclone WCBs were identified using the air mass trajectory model LAGRANTO (v2.0; Sprenger and Wernli, 2015). After calculating all cyclone tracks, LAGRANTO was applied to the ERAI fields by calculating all 48-hour air mass trajectories that start at the location of a horizontal regular grid separated by 0.5° (ranging from -15°W to 45°E and from 25°N to 50°N) and at each of the 20 equidistant pressure levels from the surface to 800 hPa. Forward trajectories were initiated every six hours (i.e. at the ERAI time steps) at least two days prior to the time of each cyclone first track point and until the time of each cyclone final track point. In this study we retained as WCBs only the air mass trajectories that rise for more than 500 hPa in 48 hours. To analyse WCBs in a climatological framework within both hemispheres, Madonna et al. (2014) applied an ascent threshold of 600 hPa. However, sensitivity tests in previous studies showed that such a threshold was rather strict for the Mediterranean cyclones, yielding WCBs composed of "few" air mass trajectories (Flaounas et al. 2015, 2016b). An ascent speed of 500 hPa in 48 hours is expected to capture the core of the WCB airstream; a lower threshold would result in more air mass trajectories composing the WCB, but risk capturing large-scale air mass ascendancies that might not correspond to a WCB.

2.2 Quantification of cyclone rainfall

To analyse the cyclones' rainfall, first we need to extract the rainfall fields that correspond to each cyclone track point. To cope with the inconsistent number of time steps between 3B42 estimates (available every 3 hours) and cyclone track points (available every 6 hours), the latter have been temporally interpolated to the missing 3-hourly time steps of the 3B42 estimates (i.e. 0300, 0900, 1500 and 2100 UTC). Attribution of rainfall to cyclones has been previously addressed by several studies (e.g. Hawcroft et al, 2012; Paprtitz et al. 2014; Flaounas et al. 2016a); in this study, we follow a similar method to Paprtitz et al. (2014). First, for each 3-hourly time step, we distinguish all non-zero rainfall grid points and group together the ones that are spatially connected. This permits identification and labelling of all different spatial structures of rainfall in a given time step. Second, we attribute to a cyclone track point any rainfall spatial structure that is located no further than 2.5° away. Figures 2a and 2b provide an example of our methodology applied to the mature stage (i.e. track point of maximum relative vorticity) of two intense cyclones that occurred in December 2005 (Fita et al. 2007) and September 2006 (Chaboureau et al. 2012), respectively. For both cyclones, their spatially-continuous rainfall fields extend to locations distant from the cyclone centres (black contour in Figs 2a and 2b), but are partly collocated with an area with a radius of 2.5° (black ellipse in Figs. 2a and 2b).

The extraction of cyclone-related rainfall has been performed for all of the tracked cyclones during the whole period 2005-2015 (i.e. for 7091 cyclones). To determine a metric that allows cyclone classification according to the magnitude of produced rainfall, we first calculated the accumulated rainfall around the cyclone centres during the whole life-time of each cyclone. As an example, Figs. 2c and 2d show the total life-time accumulated rainfall in a cyclone-centre relative grid for the two cyclone tracks in Figs. 2a and 2b, respectively. Our rainfall metric is defined as the 95th percentile of the total accumulated rainfall calculated over all grid points that received precipitation, as shown in Figs. 2c and 2d. Different rainfall metrics have been also tested, such as the maximum 3-hourly rainfall of a cyclone and the average of the cyclone's accumulated rainfall fields. However,

213 we found the one applied here is most representative for determining heavy rainfall during the whole cyclone life-cycle.

216 Figure 3a shows the relationship between maximum intensity and the rainfall metric for all 7091 cyclones. The cloud-shaped scatterplot suggests that there is no obvious mathematical relationship between the two cyclone properties. This conclusion is also valid if we only consider the most intense cyclones or the weakest ones and is
219 consistent with Pfahl and Wernli (2012) who showed that there is no apparent relationship between their cyclone track properties (such as intensity or displacement speed) and their produced extreme rainfall. However, in Fig. 3a the box and whiskers plot of rainfall metric against intensity per bin of width 2×10^{-5} s^{-1} shows that the medi-
222 ans present a clear linear relation with a correlation coefficient of 0.99 (black dashed line in Fig. 3a). Neverthe-less, the extent of the distribution outliers in Fig. 3a also shows that, regardless their intensity, cyclones present a rather large variability in rainfall metric. Especially when considering weaker cyclones, this may be partly due to
225 uncertainties in the extracted rainfall field. For instance, if a weak cyclonic feature and an intense cyclone are located close to each other, then they may share the same rainfall field. An example of such case was observed during the mature stage of the cyclone in Fig. 2b where rainfall over the Tyrrhenian sea was collocated with a
228 weaker low pressure system (Moscatello et al. 2008). On the other hand, large variability of rainfall metric in weak cyclones may be also due to strong convective cells if, e.g., tracked mesoscale vortices are formed within mesoscale convective systems (Houze, 2004). To determine the correlation between cyclones' intensity and rain-
231 fall, a different approach was also performed (not shown). Following the results of Pfahl and Sprenger (2016), cyclone maximum intensity was first scaled using the total column water vapour, averaged within 500 km from the cyclones centre and from the time of cyclogenesis until the cyclone's mature stage. Scaled intensities were
234 finally compared to rainfall averages occurring since cyclogenesis close to cyclone's centre. In contrast to the findings of Pfahl and Sprenger (2016) for extratropical cyclones, we found no significant correlation scores for the Mediterranean cyclones. A plausible explanation might reside in the sharp sea-land transitions, where the
237 influence of geographical elements might perturb total column water vapour and rainfall, as well as in the speci-ficity of Mediterranean cyclones, where convection is not common in cyclone's centre. Indeed, Galanaki et al. (2016) showed that only one third of intense Mediterranean cyclones might present lightning activity close to
240 their centre. Therefore, one could not expect for the total of Mediterranean cyclones that convection would be related to cyclones' intensification through the release of latent heat and increased rainfall due to high water va-pour content in the atmosphere.

243

In this study, we focus only on large cyclones corresponding to large-to-meso scale vortices, assuming these are most related to high-impact weather. For this reason, we limit our analysis to the 500 most intense cyclones (cor-
246 responding to the red and blue dots in Fig. 3a). Choosing the 500 most intense cyclones (about 45 cyclones per year) is consistent with the number of intense cyclones as defined by Homar et al. (2007), and also permits a ro-bust statistical analysis of cyclone-related rainfall processes. These cyclones have maximum relative vorticity
249 exceeding 16.5×10^{-5} s^{-1}, while their rainfall metric ranges from 0 to 180 mm. Figure 3b shows the probability distribution function of the 500 cyclones' rainfall metric. The distribution has a median value of about 45 mm, 24 cyclones had no rainfall at all and 12 yielded a rainfall metric exceeding 105 mm. To better understand the
252 variability of the processes that lead to heavy rainfall, we focus our study on the 250 cyclones with the highest rainfall metric (corresponding to the blue dots and blue area in Figs 3a and 3b, respectively) and eventually compare them to the 250 cyclones with lowest rainfall metric (corresponding to the red dots and red area in Figs
255 3a and 3b, respectively). Hereafter, we make the assumption that cyclones producing heavy rainfall correspond to the ones with high rainfall metrics and conveniently will refer to the two cyclone groups as those producing high and low rainfall.

258

2.3 Quantification of the cyclones' WCBs and DC contribution to rainfall
To quantify the relative contribution of DC and WCB to cyclone total rainfall, we apply the following methodol-
261 ogy to each of the 500 most intense cyclones:

a) For DC, we use lightning observations and AMSU-based diagnostics. Lightning is directly observed by
264 ZEUS, while AMSU diagnostics correspond to post-processing of satellite measurements. In fact, neither corre-sponds to a direct measurement of cloud properties or dynamics, but both are related to cloud ice content, sug-

gesting the development of DC. The AMSU diagnostic has been previously shown to be related to heavy rainfall (Funatsu et al. 2007), but has a limited temporal and spatial coverage of the Mediterranean region since its coverage depends on satellite overpasses. On the other hand, lightning observations offer an advantage in being spatially accurate and temporally continuous, but the relation of lightning impacts to DC and heavy rainfall is a rather complex issue (e.g. Avila et al. 2010). To associate the 3-hourly extracted rainfall fields to DC we treat lightning observations and AMSU diagnostics separately. Specifically, we associate the locations of all lightning impacts or AMSU diagnosed DC to the closest extracted rainfall grid point if the observations take place within a period of +/- 1.5 hours of the time of the cyclone track point (or equivalently, within the representative time window of rainfall estimates from the 3B42 algorithm).

b) For WCBs, we assume that the extracted rainfall grids from the 3B42 algorithm (available every three hours) are due to a WCB if these grid points coincide with the locations of the relevant part of WCB air mass trajectories that ranges between 800 and 400 hPa (i.e. the ascending part of the WCBs and the one typically producing most rainfall; Madonna et al, 2013). In addition, we consider that the WCB trajectories have a "width" of one grid point. Therefore, when an air mass trajectory and a 3B42 grid point coincide, we also associate to the WCB the surrounding rainfall grid points.

Figures 2e and 2f show an example of the association of extracted rainfall with lightning observations: AMSU diagnosed DC and the WCB at the time of the mature stage of the two intense cyclone cases in Figs 2a and 2b. Results show that not all rainfall grid points are attributed to the WCB or DC; however, most of the major rainfall 'hot spots' are attributable to at least one of these processes.

Reanalysis is produced by models by the assimilation of a large variety of observations and thus it is widely considered as the most credible gridded dataset for atmospheric circulation at a relatively coarse resolution. Therefore, in this study, we use ERAI to track cyclonic systems and to identify WCB airstreams. In addition, ERAI may conveniently offer continuous rainfall datasets and specific diagnostics to distinguish convective and large-scale precipitation. However, such processes are sensitive to model uncertainties linked to physics parametrizations, resolution issues and other aspects of the model configurations (e.g. Belo-Pereira et al. 2011; Szczypta et al. 2011). Therefore, our choice to use satellite and lightning observations -rather than reanalysis- to analyse DC and WCB rainfall aims to achieve a high degree of credibility in our results. Nevertheless, despite their advantage in providing a direct detection of atmospheric processes, observations may also present several limitations and may also be subject to measurement uncertainties.

Katsanos et al. (2004) assessed 3B42 rainfall estimations against raingauge data in the Mediterranean and found insignificant bias when considering low and medium rain rates. On the other hand, when accumulated rainfall exceeds 40 mm per 12 hours, 3B42 relative error might be high, with an underestimation of rainfall by up to 80%. Despite its high bias in heavy rainfall, the 3B42 product offers a great advantage in providing spatially- and temporally-continuous datasets on a relatively fine grid. Concerning ZEUS, the lightning observations are related with a location error of the order of 6.5 km, but -as all very low frequency systems- ZEUS suffers from underdetection of the actual number of lightning events. Nevertheless, ZEUS does not miss the detection of thunderstorms (Lagouvardos et al. 2009). Finally the choice of using AMSU-B/MHS is justified by the fact that convection occurrences in ERA-Interim are systematically underestimated (Alhammoud et al, 2014). DC diagnostic has been evaluated against Cloudsat data and shows a false positive percentage lower than 6 % at the global scale (Rysman et al, 2017). In addition, when compared with TRMM data, DC was found in the Mediterranean region to be related to accumulated rainfall of at least 20 mm in 3 hours in more than 50 % of the cases. This threshold was also confirmed in the Mediterranean -over surfaces free of snow or ice- with radar and rain gauges from meteorological ground stations for selected heavy precipitating events (Funatsu et al., 2007). A caveat of DC diagnostics is the discontinuous and irregular temporal sampling, depending on the daily frequency and drift of satellites passages over the Mediterranean (Claud et, 2012).

3. Intense cyclones climatology and relation to heavy rainfall
Figures 4a and 4b show the location of the mature stage of the 250 intense cyclones associated with high rainfall (blue dots in Fig. 3a) and low rainfall (red dots in Fig. 3a), respectively. Despite their differences in rainfall pro-

duction, both cyclone groups present a consistent spatial variability of occurrence. This is consistent with the results of previous intense cyclone climatologies (e.g. Trigo et al. 1999; Homar et al. 2007). In fact, cyclones in both groups reach maximum intensity over the Adriatic, the Aegean, Ionian and western Mediterranean Seas. Consistent with the analysis of the dynamics of intense Mediterranean cyclones in Flaounas et al. (2015), the majority of cyclones in Figs. 4a and 4b are located over the Mediterranean Sea, while few systems reach their maximum intensity near the Alps and the Atlas Mountains. Despite the similar spatial variability of the two cyclone groups, their seasonal cycle (Fig. 4c) shows a higher frequency of occurrence in early winter and autumn for cyclones producing high rainfall, and in spring for cyclones producing low rainfall. Climatologically, the Polar Jet is at its southern location in winter and hence Mediterranean intrusions of potential vorticity (PV) streamers are most likely to occur and in turn initiate intense cyclogenesis in this season (Fita et al. 2006; Claud et al. 2010; Flaounas et al. 2015). On the other hand, the Polar Jet is at its northern location in summer, disfavouring PV streamer intrusions. Especially in autumn, cyclones may be more likely to produce heavy rainfall due to the Mediterranean Sea surface temperature (SST), which is climatologically warmer in autumn than in winter (Dubois et al. 2012); this favours evaporation and thus potentially enhances rainfall production. The role of warmer SST in increasing intense cyclones' rainfall has been confirmed by numerical sensitivity tests (Miglietta et al. 2011; Tous et al. 2013). To highlight the importance of intense cyclones in producing heavy rainfall in the Mediterranean, we show in Figs 5a and 5b their contribution to the regional total rainfall during the years 2005-2015. The difference is striking, with cyclones yielding low rainfall (Fig. 5a) producing an average of 10% of the total 11-year Mediterranean rainfall, while those yielding high rainfall (Fig. 5b), in certain areas, producing about one third of the total. Taking into account all 500 cyclones, their total contribution is about 40%. This result is consistent with Flaounas et al. (2016a) who used 20-year regional simulations and different methodology to show that about 50% of rainfall over the Mediterranean Sea is due to intense cyclones.

4 Contribution of deep convection and warm conveyor belts to cyclone rainfall

4.1 Temporal variability

Figures 6a and 6b show the composite time series of the evolution of the cyclones' extracted rainfall, as well as the relative contribution of DC and WCBs to this rainfall. Composite time series are centred at the mature stage of the 250 cyclones producing high (Fig. 6a) and low rainfall (Fig. 6b). The 0h corresponds to each cyclone's mature stage, i.e. when the relative vorticity at the cyclone's centre is maximised. The rainfall evolution is expressed as the average percentage of 48-hour cyclone rainfall (from -24h to +24h) produced within each 3-hourly time step (where each composite 3-hourly rainfall is calculated as the average rainfall from all cyclones with available extracted rainfall at the given composite time steps). On the other hand, the contribution of lightning, AMSU-diagnosed DC and WCBs to the cyclones' rainfall is expressed as the average percentage of the total 3-hourly rainfall that overlaps with locations of lightning impacts, AMSU-diagnosed DC and the WCB, respectively (section 2.3). In addition, we show DC (magenta line in Figs 6a and 6b) considering that DC occurs when a grid point of rainfall is collocated with either lightning impacts or AMSU diagnosed DC.

In both Figs. 6a and 6b, the rainfall production tends to increase from 24h to about 6h prior to the cyclone mature stage (i.e. until -6h). Then, within six hours, from -6h to 0h, cyclones in both cyclone groups tend to produce on average about 30% of their total 48-hour rainfall. Thereafter, rainfall production decreases smoothly. In cyclones producing high rainfall (Fig. 6a), the contribution of DC (magenta line) and WCBs (blue line) to rainfall increases in parallel with rainfall production (black line) from -24h to -6h. Then, from -6h to 0h, when most rainfall is produced, the WCB contributes about 50%, while DC contributes about 15 to 20%. Such strong contribution of WCBs to cyclone rainfall is consistent with the climatological results of Pfahl et al. (2014) and with the five cyclone case analyses in Raveh and Wernli (2016). In cyclones producing low rainfall, the contribution of WCBs (Fig. 6b) tends to present a similar variability to that for cyclones producing high rainfall (Fig. 6a), but with lower percentage. On the other hand, the contribution of DC to rainfall shows a rather weak variability for these low-rainfall cyclones, being quasi-constant from -12h to +12h (Fig. 6b) rather than reaching a clear maximum at around -6h as in cyclones producing high rainfall (Fig. 6a).

The total contribution of the WCB and DC to rainfall differs in the two cyclone groups. For instance, at -6h the two processes explain about 70% of the rainfall of cyclones with high rainfall (Fig. 6a), but only 50% of the rain-

372 fall of cyclones with low rainfall (Fig. 6b). Thus, this analysis shows that the WCB and DC are the dominant processes through which intense Mediterranean cyclones produce heavy rainfall. On the other hand, the considerable residual suggests that DC and the WCB do not explain all of the rainfall of cyclones with high rainfall.

375 Lightning observations and reanalysis data are continuously available throughout the 11-year period (only AMSU diagnostics present missing values when no satellites pass over the Mediterranean) and hence it is rather unlikely that the rainfall residual is due to incomplete spatial and temporal coverage of the observations. Conse-

378 quently, part of this residual may be attributed to inconsistencies between 3B42 rainfall estimates, observations and reanalysis data (e.g. misplaced 3B42 fields with respect to observations), but the largest part is most probably related to undiagnosed atmospheric processes (processes other than DC and the WCB) that take place over

381 both land and sea. Indeed, Raveh and Wernli (2016) showed that shallow convection and orography interactions with the atmospheric flow may contribute significantly to heavy rainfall in cyclones. The Mediterranean basin has a complex geography (Fig. 1) with several intense cyclones reaching their mature stage close to or over land

384 (Fig. 4). In fact, our analysis shows that about 50 to 60% of cyclone total extracted rainfall is produced over land, regardless of whether DC or WCBs are also present. Due to the complex nature of orographically-induced rainfall here we do not treat explicitly rainfall over land as a unique process since several different underlying

387 atmospheric processes may be implicated, especially when considering orographically-forced convection (e.g. Cannon et al. 2012; Barrett et al. 2015).

390 **4.2 Spatial variability**

In this section we focus only on cyclones producing high rainfall. Figure 7 shows the spatial variability of rainfall, WCB and DC at the times of the cyclones' intensifying stage (-12h), when cyclone intensity is maximum

393 (0h) and during their decay phase (+12h). Spatial variabilities are calculated in cyclone-centre relative locations and are expressed as the average, over the 250 cyclones, occurrence of rainfall, lightning and DC (as diagnosed by AMSU observations) at each grid point.

396

The highest probabilities of rainfall occurrence (Fig. 7, top panels) are located close to cyclone centres, while areas affected by rainfall extend from 5° west to cyclone centres to 7.5° east. In particular, rainfall occurrence is

399 favoured at the north-east side of cyclone centres, regardless of the stage in the cyclone lifecycle. This result is consistent with Flaounas et al. (2015) who reached similar results, but using a regional climate simulation. In the middle panels of Fig. 7, lightning and the AMSU-diagnostic yield similar spatial patterns, suggesting that DC

402 tends to take place close to cyclone centres most probably due to convection in their fronts. A characteristic example is shown in Fig. 2a, where 3-hourly rainfall of more than 40 mm takes place alongside the cyclone's cold front (not shown) to the east of the cyclone centre (at 20°E-35°N). Figure 2e confirms that this region is strongly

405 characterized by lightning activity and AMSU-diagnosed DC. Concerning rainfall produced by the WCB (Fig. 7, bottom panels), more than 40% of occurrences are located to the north of cyclone centres. Especially at +12h, the WCBs produce rainfall within a rainband that expands zonally from 2.5° west of cyclone centres to 10° to

408 their east. This rainband has a similar spatial structure to that of the characteristic comma-shaped cloud of extratropical cyclones. Similar spatial structure of rainfall at times subsequent to that of cyclone maximum intensity has been also found by Flaounas et al. (2015). In fact, the WCB typically rises from the lower atmospheric levels

411 to the upper troposphere within 48 hours. As a result, the moist air masses that rise over the warm fronts during the cyclone mature stage (at 0h) may continue to contribute to cyclone rainfall at later times.

414 In Fig. 7, the areas where DC and WCB rainfall are favoured present a fairly limited overlapping. In particular, WCBs initiate rainfall in northern locations and close to the cyclone centres, while DC takes place close to the cyclone centres and towards the east. This is consistent with Raveh-Rubin and Wernli (2016) who showed that

417 rainfall takes place in locations to the north and east of cyclone centres and that DC is favoured along the cyclone's fronts and close to the cyclone's centre. In fact, about 8% of rainfall grid points that present WCBs overlap with rainfall grid points associated to either lightning or AMSU-diagnosed DC. On the other hand, about

420 30% of rainfall grid points that present either lightning or AMSU-diagnosed DC overlap with rainfall grid points due to WCBs. This suggests that a considerable percentage of DC forms part of the embedded convection in WCBs. Indeed, previous studies showed that WCBs have been associated with both convective and large-scale

423 precipitation (Martinez-Alvarado et al, 2014; Rasp et al, 2016). The limited overlapping between the areas affected by DC and the WCB was also observed in the detailed analysis of a cyclone case study (Flaounas et al.

2016b, their figure 6). It is noteworthy that the atmospheric fields in Fig. 7 were not rotated about cyclone centres to yield composite averages with coherent frontal structures. Rotated composite fields were previously used by Merill (1988) and more recently by Catto et al. (2010) and Martínez-Alvarado et al. (2012). Rotation would result in Fig. 7 presenting a more robust spatial structure of lightning and AMSU-diagnosed DC occurrence. Regardless of the fields' rotation, our rainfall composites are consistent with the rotated ones in Flaounas et al. (2015), while our composite DC and WCB locations are consistent with the ones found in the five cyclone analysis of Raveh-Rubin and Wernli (2016).

4.3 Rainfall relation to lightning impacts and number of WCB trajectories

In the previous sections we showed that DC and WCBs are associated with the largest part of cyclones' high rainfall and WCBs may potentially produce about half of the rainfall when cyclones reach their mature stage. To complement our results on the spatio-temporal variability of DC and WCBs producing cyclones' rainfall, in this section we address the relationship of rainfall intensity to lightning impacts and the number of WCB air mass trajectories. In Figs 8a and b we present the boxplots of the distribution of lightning impacts and the number of WCB trajectories, respectively, per 3-hourly rainfall bins of a width of 5 mm. To produce Fig. 8 we took into account only the cyclone rainfall grid points that present solely lightning or WCB trajectories above the Mediterranean Sea. This was done to avoid complex interactions between orography and air flow which would potentially influence the rainfall amount. Finally, we calculated distributions only for bins that include at least 100 events. In Fig. 8a, the 3-hourly rainfall median and the 75th and the 95th quantiles increase with the logarithm of the number of lightning impacts. On the other hand, in Fig. 8b, the median and the 75th and 95th quantile of the number of trajectories of WCBs increase in parallel with rainfall only until about 35 mm. In contrast, the 25th and 5th quantile of each bin boxplot for both lightning and WCBs present a less consistent relationship with rainfall. We hypothesise that there is a relationship that bounds the maximum number of lightning impacts or WCB trajectories that can occur to yield a certain rainfall amount, but there is no relationship for their minimum number. Consequently, the same rainfall amounts may occur even with few lightning impacts or few WCB trajectories. In fact, associating rainfall to simple properties such as the number of lightning impacts and WCB trajectories is a delicate issue since more factors are implicated in rainfall production, for instance the air masses' water content, the precipitation efficiency of an atmospheric system and the degree of atmospheric instability. Nevertheless, Fig. 8 clearly shows that DC may be associated with significantly higher rainfall intensities than WCBs

5. Summary and conclusions

A climatological dataset of intense Mediterranean cyclones has been analysed, focusing on the 500 most intense cyclones of the period 2005-2015. For each cyclone, we extracted the associated rainfall field and defined a metric to determine the magnitude of produced rainfall (defined as the 95th quantile of rainfall of the cyclone's total life time accumulated rainfall field grid points). Then, we applied a diagnostic methodology to attribute and quantify the rainfall produced by DC and the WCB. To diagnose rainfall due to DC, we directly related observations to rainfall estimations while, for the WCB, we attributed rainfall to the locations where air mass trajectories tend to rise, from 800 to 400 hPa. In the following, we reply to the questions raised in the introduction:

- In a first step, we associated the rainfall and maximum intensity of all tracked cyclones. The results showed a rather large variability, demonstrating that even the most intense cyclones may produce low rainfall amounts. Despite this variability, a linear relationship was found when comparing the median of the cyclones' rainfall to their maximum intensity. Focusing only on the 500 most intense cyclones we found a median rainfall metric value of about 45mm. This was used as a threshold to distinguish two cyclone groups: the 250 intense cyclones producing low rainfall and the 250 cyclones producing high rainfall. The former group was found to produce about 10% of the total Mediterranean rainfall, while the latter produced about 30%. Furthermore, we found that the intense cyclones producing high rainfall tend to occur in autumn and winter, while the cyclones producing low rainfall tend to mostly occur in spring.

- Composite time series of rainfall production showed that all 500 cyclones tended to produce on average about 30% of their 48-hour rainfall within the six hours prior to their mature stage, i.e. from -6h to 0h. Using observations and trajectory analysis, we distinguished and quantified the relative contribution of DC and the WCB to the cyclones' rainfall during this period. In particular, to extract rainfall due to WCBs, we retained only rainfall grids

that coincide with the locations of air mass trajectories that present an ascent of at least 500 hPa in 48 hours and are located between 800 and 400 hPa. For cyclones producing high rainfall, results showed that WCBs contribute up to about 50% of rainfall, while DC was found to contribute up to about 20%. On the other hand, for cyclones producing low rainfall, WCBs contributed up to 40% of rainfall, while DC contributed no more than about 10%. These results show that DC and the WCB are the dominant processes through which cyclones produce high rainfall (reaching a total maximum contribution of about 70%).

- Furthermore, we showed that the development of DC is favoured close to cyclone centres and towards their eastern side, most probably due to the system fronts. On the other hand, the WCB tends to produce rainfall on the north east side of cyclone centres. We found only 8% of DC collocated with WCBs, suggesting that these two processes are dissociated in cyclones producing heavy rainfall. Nevertheless, about 30% of rainfall grid points associated with DC overlap with the ones associated with WCBs suggesting that a significant part of DC corresponds to embedded convection in WCBs. Finally, we showed that the number of lightning and trajectories corresponding to the WCB tends to increase with rainfall rain rates. Nevertheless, it seems that relatively high rain rates (more than 50 mm in 3 hours) are most likely to occur due to DC rather than due to the WCB.

In this study, we applied several diagnostic methodologies combining reanalysis data with observations. Consequently, there may be uncertainties associated with some aspects of our results (e.g. relating air mass trajectories with rainfall estimations from TRMM). Nevertheless, we provided an insight to the spatio-temporal variability of DC and the WCB, quantifying their relative contribution to cyclone rainfall. Our results complement previous studies on the role of DC and the WCB to produce heavy rainfall. Most importantly, we quantified in a climatological framework the relative contribution of these processes and showed their relationship with cyclone rainfall. In future studies we will address the question of cyclone water budget and dynamical life cycle to gain a better understanding of the cyclone mechanisms leading to heavy rainfall.

References
Alhammoud B, Claud C, Funatsu, BM, Béranger K, Chaboureau JP (2014) Patterns of Precipitation and Convection Occurrence over the Mediterranean Basin Derived from a Decade of Microwave Satellite Observations. Atmosphere 5:370-398

Avila EE, Bürgesser RE, Castellano NE, Collier AB, Compagnucci RH, Hughes AR (2010) Correlations between deep convection and lightning activity on a global scale. J Atmos Sol-Terr Phys 72(14):1114-1121

Barrett AI, Gray SL, Kirshbaum DJ, Roberts NM, Schultz DM, Fairman JG (2015) Synoptic versus orographic control on stationary convective banding. Q J R Meteorol Soc 141:1101–113. doi:10.1002/qj.2409

Belo-Pereira M, Dutra E, Viterbo P (2011) Evaluation of global precipitation data sets over the Iberian Peninsula. J Geophys Res Atmos 116:D20101. doi:10.1029/2010JD015481.

Čampa J, Wernli H (2012) A PV Perspective on the Vertical Structure of Mature Midlatitude Cyclones in the Northern Hemisphere J Atmos Sci 69:725–740. doi:10.1175/JAS-D-11-050.1

Campins J, Jansà A, Genovés A (2006) Three-dimensional structure of western Mediterranean cyclones. Int J Climatol 26:323–343. doi:10.1002/joc.1275

Cannon DJ, Kirshbaum DJ, Gray SL (2012) Under what conditions does embedded convection enhance

orographic precipitation?. Q J R Meteorol Soc 138:391–406. doi:10.1002/qj.926

Catto JL, Shaffrey LC, Hodges KI (2010) Can Climate Models Capture the Structure of Extratropical Cyclones?. J Clim 23:1621–1635. doi:10.1175/2009JCLI3318.1

Chaboureau JP, Pantillon F, Lambert D, Richard E, Claud C (2012) Tropical transition of a Mediterranean storm by jet crossing. Q J R Meteorol Soc *138*(664): 596-611

Claud C, Alhammoud B, Funatsu BM, Chaboureau JP (2010) Mediterranean hurricanes: large-scale environment and convective and precipitating areas from satellite microwave observations. Nat Hazards Earth Syst Sci 10:2199-2213. doi:10.5194/nhess-10-2199-2010

Claud C, Alhammoud B, Funatsu BM, Lebeaupin Brossier C, Chaboureau JP, Béranger K, Drobinski P (2012) A high resolution climatology of precipitation and deep convection over the Mediterranean region from operational satellite microwave data: development and application to the evaluation of model uncertainties. Nat Hazards Earth Syst Sci 12:785-798. doi:10.5194/nhess-12-785-2012

Davolio S, Miglietta MM, Moscatello A, Pacifico F, Buzzi A, Rotunno R (2009) Numerical forecast and analysis of a tropical-like cyclone in the Ionian Sea. Nat Hazards Earth Syst Sci 9(2):551-562

Dee DP, Uppala SM, Simmons AJ, Berrisford P, Poli P, Kobayashi S, Andrae U, Balmaseda MA, Balsamo G, Bauer P, Bechtold P, Beljaars ACM, van de Berg L, Bidlot J, Bormann N, Delsol C, Dragani R, Fuentes M, Geer AJ, Haimberger L, Healy SB, Hersbach H, H_olm EV, Isaksen L, K_allberg P, K• ohler M, Matricardi M, McNally AP, Monge-Sanz BM, Morcrette JJ, Park BK, Peubey C, de Rosnay P, Tavolato C, Th_epaut JN, Vitart F (2011) The ERA-interim reanalysis: con_guration and performance of the data assimilation system. Q J R Meteorol Soc 137(656):553-597. DOI:10.1002/qj.828

Dubois C, Somot S, Calmanti S, Carillo A, Déqué M, Dell'Aquilla A, Elizalde A, Gualdi S, Jacob D, L'hévéder B, Li L (2012) Future projections of the surface heat and water budgets of the Mediterranean Sea in an ensemble of coupled atmosphere–ocean regional climate models. Clim Dyn 39(7-8):1859-84

Fita L, Romero R, Ramis C (2006) Intercomparison of intense cyclogenesis events over the Mediterranean basin based on baroclinic and diabatic influences. Adv Geosci 7:333-342

Fita L, Romero R, Luque A, Emanuel K, Ramis C (2007) Analysis of the environments of seven Mediterranean tropical-like storms using an axisymmetric, nonhydrostatic, cloud resolving model. Nat. Hazards Earth Syst Sci 7:41-56. doi:10.5194/nhess-7-41-2007

Flaounas E, Kotroni V, Lagouvardos K, Flaounas I (2014) CycloTRACK (v1.0) – tracking winter extratropical cyclones based on relative vorticity: sensitivity to data filtering and other relevant parameters. Geosci Model Dev 7:1841-1853. doi:10.5194/gmd-7-1841-2014

Flaounas E, Raveh-Rubin S, Wernli H, Drobinski P, Bastin S (2015) The dynamical structure of intense Mediterranean cyclones. Clim Dyn 44(9-10): 2411-2427

Flaounas E, Di Luca A, Drobinski P, Mailler S, Arsouze T, Bastin S, Beranger K, Lebeaupin Brossier C (2016a) Cyclone contribution to the Mediterranean Sea water budget. Clim Dyn 46(3-4): 913-927

Flaounas E, Lagouvardos K, Kotroni V, Claud C, Delanoë J, Flamant C, Madonna E, Wernli H (2016b) Processes leading to heavy precipitation associated with two Mediterranean cyclones observed during the HyMeX SOP1. Q J R Meteorol Soc 142:275–286. doi:10.1002/qj.2618

Flaounas E, Kelemen FD, Wernli H, Gaertner MA, Reale M, Sanchez-Gomez E, Lionello P, Calmanti S,

585 Podrascanin Z, Somot S, Akhtar N, Romera R, Conte D (2017) Assessment of an ensemble of ocean-atmosphere coupled and uncoupled regional climate models to reproduce the climatology of Mediterranean cyclones. Clim Dyn 1–18. doi:10.1007/s00382-016-3398-7

588 Funatsu BM, Claud C, Chaboureau JP (2007) Potential of Advanced Microwave Sounding Unit to identify precipitating systems and associated upper-level features in the Mediterranean region: Case studies. J Geophys Res 112:D17113. doi:10.1029/2006JD008297

591

Galanaki E, Flaounas E, Kotroni V, Lagouvardos K, Argiriou A (2016) Lightning activity in the Mediterranean: quantification of cyclones contribution and relation to their intensity. Atmos Sci Lett. doi:10.1002/asl.685

594

Grams CM, Wernli H, Böttcher M, Čampa J, Corsmeier U, Jones SC, Keller JH, Lenz CJ, Wiegand L (2011) The key role of diabatic processes in modifying the upper-tropospheric wave guide: a North Atlantic case-study.
597 Q J R Meteorol Soc 137:2174–2193. doi:10.1002/qj.891

Hawcroft MK, Shaffrey LC, Hodges KI, Dacre HF (2012) How much Northern Hemisphere precipitation is as-
600 sociated with extratropical cyclones?. Geophys Res Lett 39:L24809. doi:10.1029/2012GL053866

Homar V, Jansà A, Campins J, Genovés A, Ramis C (2007) Towards a systematic climatology of sensitivities of
603 Mediterranean high impact weather: a contribution based on intense cyclones. Nat Hazards Earth Syst Sci 7(4):445-454

606 Hong G, Heygster G, Miao J, Kunzi K (2005) Detection of tropical deep convective clouds from AMSU- B water vapor channels measurements. J Geophys Res Atmos 110(D5)

609 Houze RA (2004) Mesoscale convective systems. Rev Geophys 42(4)

Huffman GJ, Bolvin DT, Nelkin EJ, Wolff DB, Adler RF, Gu G, Hong Y, Bowman KP, Stocker EF (2007) The
612 TRMM Multisatellite Precipitation Analysis (TMPA): Quasi-Global, Multiyear, Combined-Sensor Precipitation Estimates at Fine Scales. J Hydrometeorol 8:38–55. doi:10.1175/JHM560.1.

615 Katsanos D, Lagouvardos K, Jansa A, Genoves A, Picornell M, Campins J, Riosalido R, Carretero O (2001) Western Mediterranean cyclones and heavy rain. Part 2: Statistical approach. Meterol Appl 8(1):43-56

618 Kotroni V, Lagouvardos K, Kallos G, Ziakopoulos D (1999) Severe flooding over central and southern Greece associated with pre-cold frontal orographic lifting. Q J R Meteorol Soc 125:967-991

621 Kotroni V, Huffmann GJ (2004) Statistical evaluation of MPA- RT high- resolution precipitation estimates from satellite platforms over the central and eastern Mediterranean. Geophys Res Lett 31(6). doi:10.1029/2003GL019142.

624

Kotroni V, Lagouvardos K (2008) Lightning occurrence in relation with elevation, terrain slope and vegetation cover over the Mediterranean. J Geophys Res 113:D21118. doi:10.1029/2008JD010605

627

Kotroni V, Lagouvardos K (2016) Lightning in the Mediterranean and its relation with sea-surface temperature. Environ Res Lett 11:034006

630

Lagouvardos K, Kotroni V, Dobricic S, Nickovic S, Kallos G (1996) The storm of October 21–22, 1994, over Greece: Observations and model results. J Geophys Res 101(D21):26217–26226, doi:10.1029/96JD01385

633

Lagouvardos K, Kotroni V, Defer E (2007a) The 21–22 January 2004 explosive cyclogenesis over the Aegean Sea: observations and model analysis. Q J R Meteorol Soc 133(627):1519-1531

636

Lagouvardos K, Kotroni V (2007b) TRMM and lightning observations of a low-pressure system over the Eastern Mediterranean. Bull Am Meteorol Soc 88(9):1363

Lagouvardos K, Kotroni V, Betz HD, Schmidt K (2009) A comparison of lightning data provided by ZEUS and LINET networks over Western Europe. Nat Hazards Earth Syst Sci 9:1713-1717

Lionello P, Bhend J, Buzzi A, Della-Marta PM, Krichak SO, Jansà A, Maheras P, Sanna A, Trigo IF, Trigo R (2006) Chapter 6 Cyclones in the Mediterranean region: Climatology and effects on the environment, In: P. Lionello, P. Malanotte-Rizzoli and R. Boscolo, Editor(s), Developments in Earth and Environmental Sciences, Elsevier, 2006, Volume 4, Pages 325-372, ISSN 1571-9197, ISBN 9780444521705

Lionello P, Trigo I, Gil V, Liberato M, Nissen K, Pinto J, Raible C, Reale M, Tanzarella A, Trigo R, Ulbrich S, Ulbrich U (2016) Objective climatology of cyclones in the Mediterranean region: a consensus view among methods with different system identification and tracking criteria. Tellus A 68. doi:10.3402/tellusa.v68.29391

Llasat-Botija M, Llasat MC, López L (2007) Natural hazards and the press in the western Mediterranean region. Adv Geosci 12:81-85

Madonna E, Wernli H, Joos H, Martius O (2014) Warm conveyor belts in the ERA-Interim dataset (1979–2010). Part I: Climatology and potential vorticity evolution. J Clim 27(1):3-26

Martínez-Alvarado O, Gray SL, Catto JL, Clark PA (2012) Sting jets in intense winter North-Atlantic windstorms. Environ Res Lett 7:024014

Martinez-Alvarado O, Joos H, Chagnon J, Boettcher M, Gray SL, Plant RS, Methven J, Wernli H (2014) The dichotomous structure of the warm conveyor belt. Q J R Meteorol Soc 140:1809-1824.

McTaggart-Cowan R, Galarneau Jr TJ, Bosart LF, Milbrandt JA (2010) Development and Tropical Transition of an Alpine Lee Cyclone. Part I: Case Analysis and Evaluation of Numerical Guidance. Mon Weather Rev 138:2281–2307. doi:10.1175/2009MWR3147.1

Merrill RT (1988) Characteristics of the Upper-Tropospheric Environmental Flow around Hurricanes. J Atmos Sci 45:1665–1677, doi 10.1175/1520-0469(1988)045<1665:COTUTE>2.0.CO;2

Miglietta MM, Moscatello A, Conte D, Mannarini G, Lacorata G, Rotunno R (2011) Numerical analysis of a Mediterranean 'hurricane' over south-eastern Italy: sensitivity experiments to sea surface temperature. Atmos Res 101(1):412-426

Miglietta MM, Laviola S, Malvaldi A, Conte D, Levizzani V, Price C (2013) Analysis of tropical- like cyclones over the Mediterranean Sea through a combined modeling and satellite approach. Geophys Res Lett 40(10):2400-2405

Moscatello A, Miglietta MM, Rotunno R (2008) Observational analysis of a Mediterranean "hurricane" over southeastern Italy. Weather 63: 306-311.

Nissen KM, Leckebusch GC, Pinto JG, Renggli D, Ulbrich S, Ulbrich U (2010) Cyclones causing wind storms in the Mediterranean: characteristics, trends and links to large-scale patterns. Nat Hazards Earth Syst Sci 10(7):1379-1391

Papritz L, Pfahl S, Rudeva I, Simmonds I, Sodemann H, Wernli H (2014) The Role of Extratropical Cyclones and Fronts for Southern Ocean Freshwater Fluxes. J Clim 27:6205–6224. doi:10.1175/JCLI-D-13-00409.1

Romilly TG, Gebremichael M (2011) Evaluation of satellite rainfall estimates over Ethiopian river basins. Hy-

690   drol Earth Syst Sci 15(5):1505

Pfahl S, Wernli H (2012) Quantifying the Relevance of Cyclones for Precipitation Extremes. J Clim 25:6770–
693   6780. doi:10.1175/JCLI-D-11-00705.1

Pfahl S, Madonna E, Boettcher M, Joos H, Wernli H (2014) Warm conveyor belts in the ERA-Interim dataset
696   (1979–2010). Part II: Moisture origin and relevance for precipitation. J Clim 27(1):27-40

Pfahl S, Sprenger M (2016) On the relationship between extratropical cyclone precipitation and intensity. Ge-
699   ophys Res Lett 43:1752–1758. doi:10.1002/2016GL068018

Pinto J, Ulbrich S, Economou T, Stephenson D, Karremann M, Shaffrey L (2016) Robustness of serial clustering
702   of extratropical cyclones to the choice of tracking method. *Tellus A, 68.* doi:10.3402/tellusa.v68.32204

Rasp S, Selz T, Craig GC (2016) Convective and slantwise trajectory ascent in convection-permitting simula-
705   tions of midlatitude cyclones. Mon Weather Rev 144:3961-3975.

Raveh-Rubin S, Wernli H (2015) Large-scale wind and precipitation extremes in the Mediterranean: a climato-
708   logical analysis for 1979–2012. Q J R Meteorol Soc 141(691):2404-2417

Raveh-Rubin S, Wernli H (2016) Large-scale wind and precipitation extremes in the Mediterranean: dynamical
711   aspects of five selected cyclone events. Q J R Meteorol Soc 142: 3097–3114. doi:10.1002/qj.2891

Romero R (2001) Sensitivity of a heavy- rain- producing western Mediterranean cyclone to embedded poten-
714   tial- vorticity anomalies. Q J R Meteorol Soc 127(578):2559-2597

Rudeva I, Gulev SK, Simmonds I, Tilinina N (2014) The sensitivity of characteristics of cyclone activity to iden-
717   tification procedures in tracking algorithms. Tellus A 66:24961. doi:10.3402/tellusa.v66.24961

Rysman JF, Claud C, Chaboureau JP, Delanoë J, Funatsu BM (2015) Severe convection in the Mediterranean
720   from microwave observations and a convection- permitting model. Q J R Meteorol Soc 142:43–55.
        doi:10.1002/qj.2611

723   Rysman JF, Claud C, Delanoë J (2017) Monitoring Deep Convection and Convective Overshooting From 60° S to
        60° N Using MHS: A Cloudsat/CALIPSO-Based Assessment. IEEE Geosci Remote S, 14(2), 159-163.

726   Szczypta C, Calvet JC, Albergel C, Balsamo G, Boussetta S, Carrer D, Lafont S, Meurey C (2011) Verification
        of the new ECMWF ERA-Interim reanalysis over France. Hydrol Earth Syst Sci 15:647-666. doi:10.5194/hess-
        15-647-2011
729

Romero R (2001) Sensitivity of a heavy- rain- producing western Mediterranean cyclone to embedded poten-
        tial- vorticity anomalies. Q J R Meteorol Soc 127(578):2559-2597
732

Sprenger M, Wernli H (2015) The LAGRANTO Lagrangian analysis tool–version 2.0. Geosci Model Dev
        8(8):2569-2586
735

Tous M, Romero R, Ramis C (2013) Surface heat fluxes influence on medicane trajectories and intensification.
        Atmos Res 123:400-411
738

Trigo IF, Davies TD, Bigg GR (1999) Objective climatology of cyclones in the Mediterranean region. J Clim
        12(6):1685-1696
741

Trigo IF (2006) Climatology and interannual variability of storm-tracks in the Euro-Atlantic sector: a compari-

son between ERA-40 and NCEP/NCAR reanalyses. Clim Dyn 26:127. doi:10.1007/s00382-005-0065-9

Ziv B, Saaroni H, Romem M, Heifetz E, Harnik N, Baharad A (2010) Analysis of conveyor belts in winter Mediterranean cyclones. Theor Appl Climatol 99:441. doi:10.1007/s00704-009-0150-9

744

747

750

753

756

Figures

759
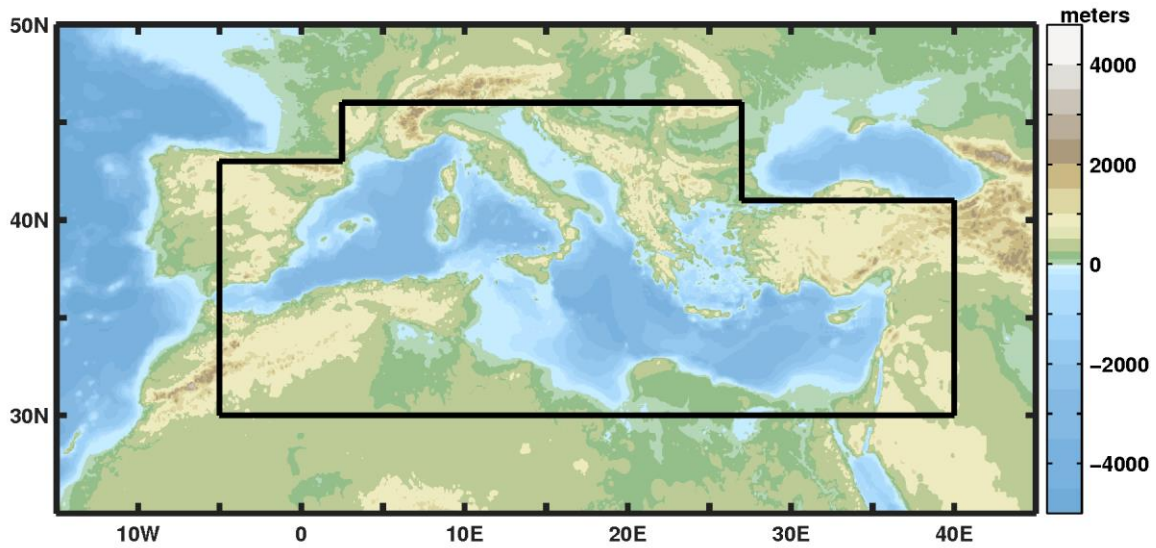
Fig. 1 Topography of the Mediterranean basin. Cyclone tracks have been retained if their mature stage is located
762 within the area outlined by the *black lines*.

765

768

771
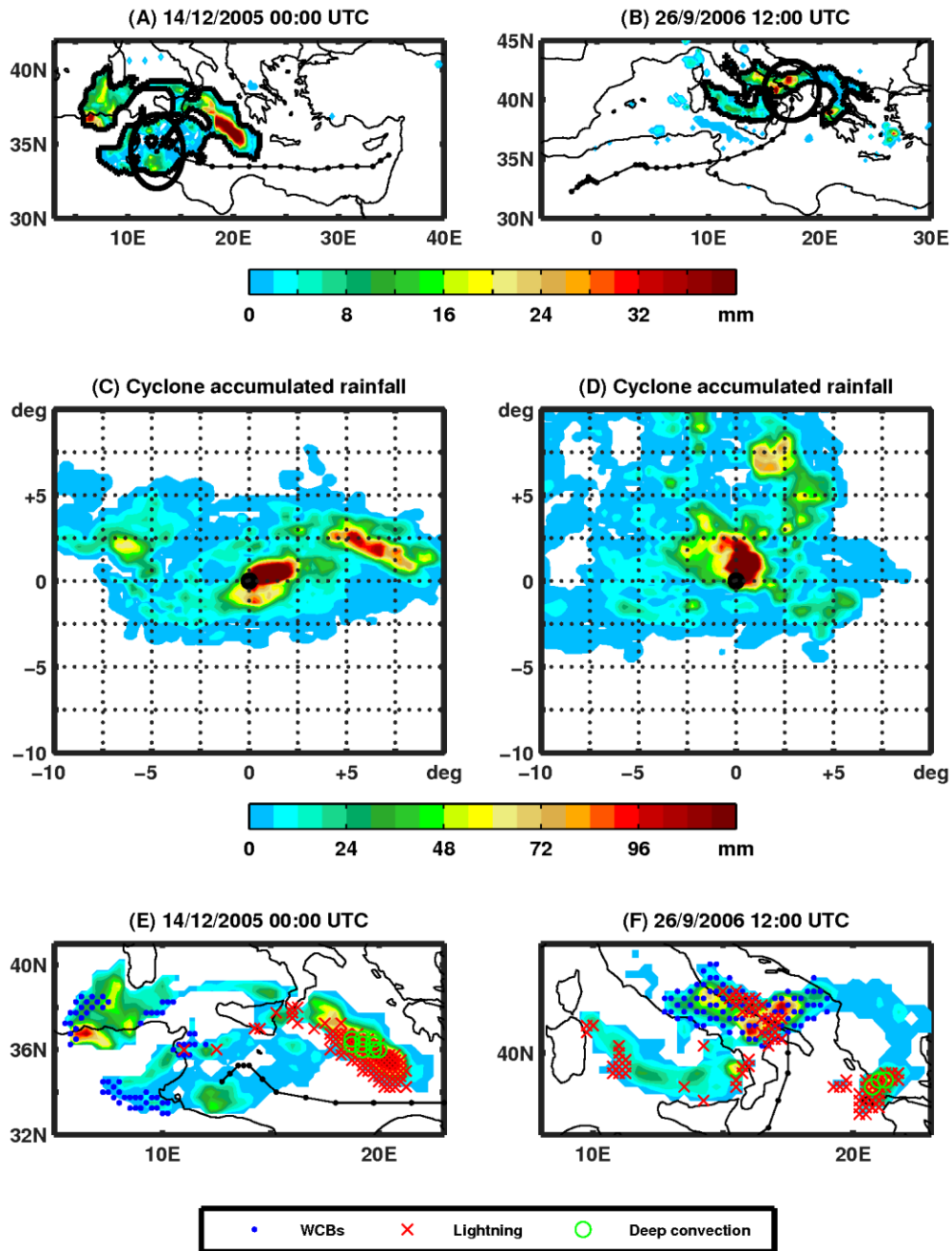
Fig. 2 (A) Three-hourly accumulated rainfall (in *colour*) at the time of an intense cyclone maximum intensity, at 0000 UTC on 14 December 2005. *Black line* depicts the cyclone's trajectory and *black circle* depicts a 2.5° area around its centre. *Black contour* outlines the rainfall field associated with the cyclone. **(B)** As in **(A)** but for the cyclone's maximum intensity occurring at 1200 UTC on 26 September 2006. **(C)** and **(D)** Total accumulated rainfall with respect to the cyclone's centre in **(A)** and **(B)**, respectively. **(E)** and **(F)** Cyclone-related three-hourly accumulated rainfall (in *colour*), as outlined by the *black contour* in **(A)** and **(B)**, respectively. *Blue dots, red crosses* and *green circles* depict rainfall grid points related to WCBs, lightning impacts and AMSU-diagnosed DC, respectively.
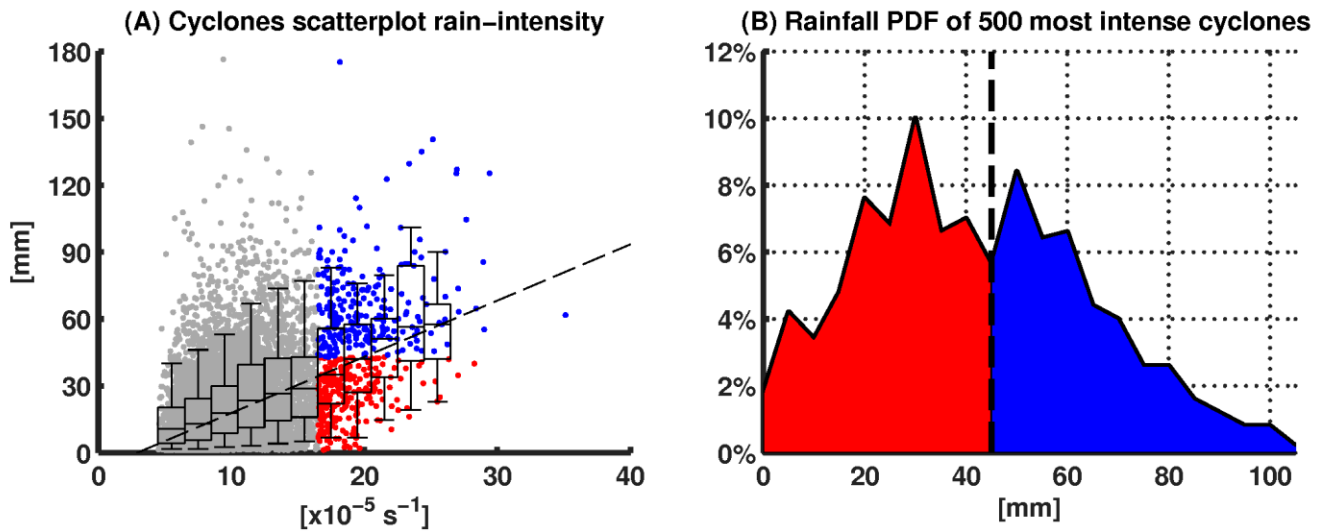
Fig. 3 (A) Scatterplot relating all tracked cyclones rainfall metric (95th quantile of the total life time accumulated rainfall field grid points) with their maximum intensity (in *dots*). Out of the 500 most intense cyclones, *Blue dots* (*Red dots*) correspond to the 250 cyclones presenting most (least) rainfall. *Boxplots* denote the distributions of rainfall metric per bin of intensity (bins width is equal to 2×10-5 s-1). Whiskers denote the 5th and 95th quantile. *Dashed line* shows the linear regression of the distributions' median. **(B)** Probability distribution function of rainfall metric for the 500 most intense cyclones. *Red* and *Blue areas* correspond to the distribution of cyclones depicted by *red* and *blue dots* in **(A)**. The areas are divided by the distribution's median (*dashed line* at 45 mm).

(A) 250 cyclones producing low rainfall

(B) 250 cyclones producing high rainfall

(C) Intense cyclones Seasonal cycle

798
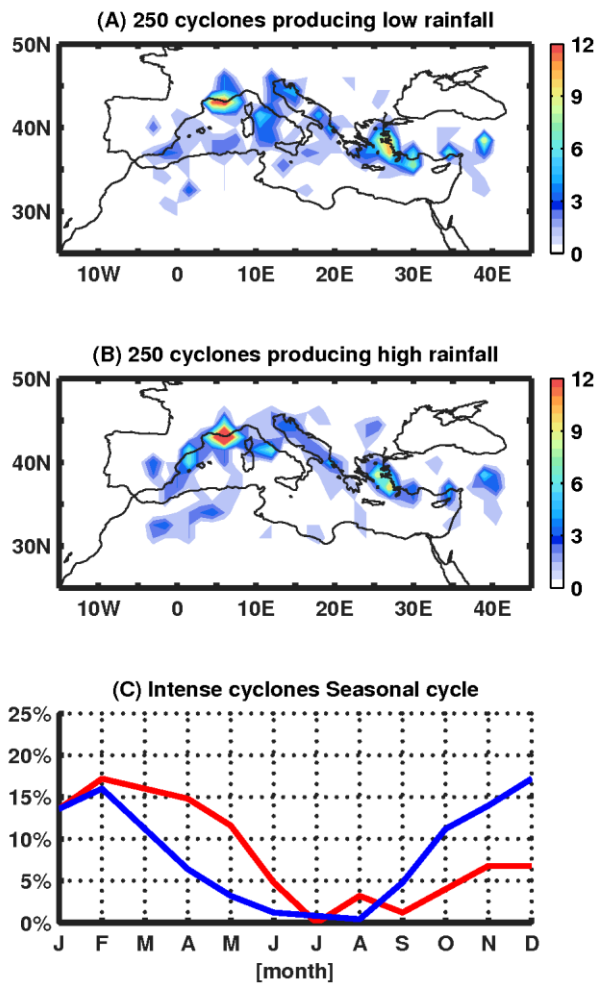
Fig. 4 (A) Spatial variability of occurrence for the mature stage of the 250 most intense cyclones producing low rainfall, expressed in number of cyclones per 2.5° (in *colour*). **(B)** As in **(A)** but for the 250 most intense cyclones that produce high rainfall. **(C)** Seasonal cycle of occurrence for the 250 intense cyclones producing low rainfall (*red line*) and for the 250 intense cyclones producing high rainfall (*blue line*).

801

804

(A) 250 intense cyclones producing low rainfall

(B) 250 intense cyclones producing high rainfall
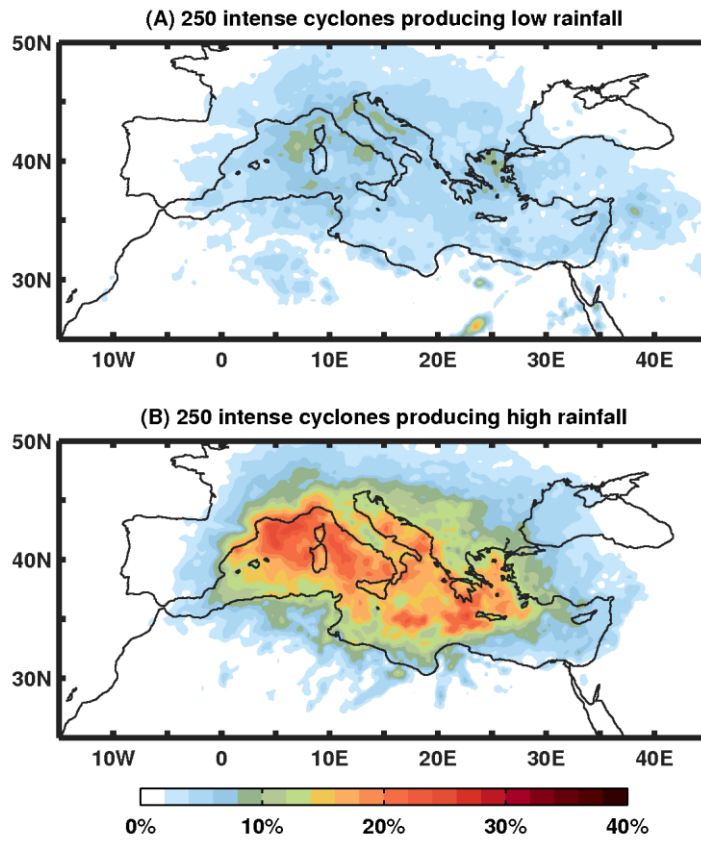
807 **Fig. 5 (A)** Percentage of the total rainfall during the period 2005-2015 due to the 250 intense cyclones producing least rainfall. **(B)** As in **(A)** but for the 250 intense cyclones producing most rainfall.

810

813

816
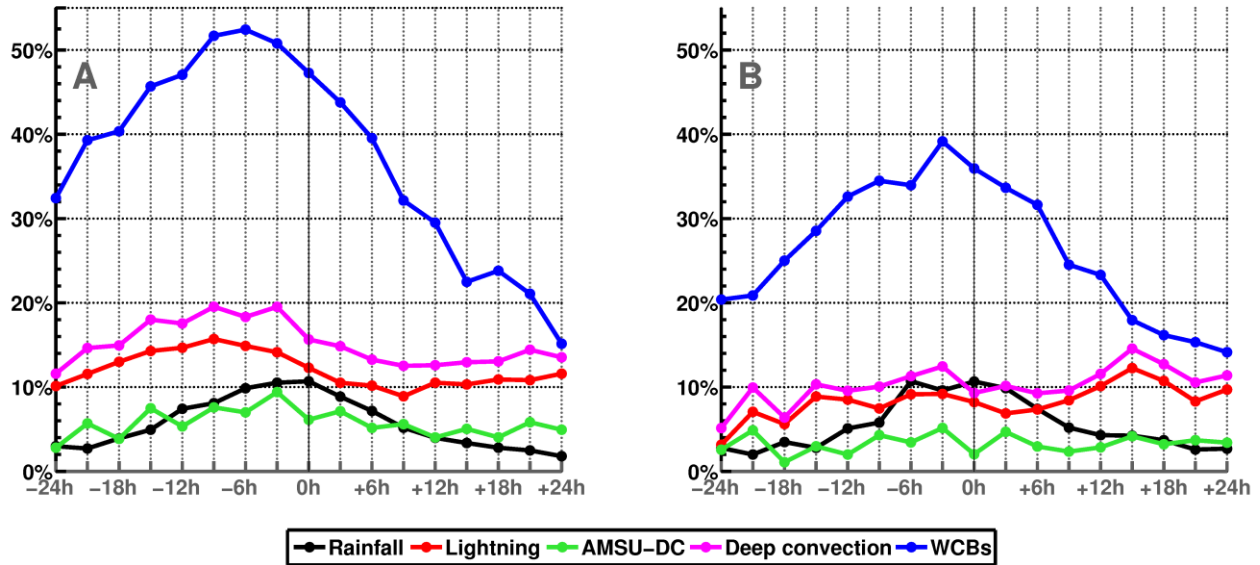
Fig. 6 (A) Composite time series, averaged for the 250 intense cyclones producing high rainfall. Time series are centred in time such that 0h corresponds to the cyclone's track point with maximum relative vorticity. *Black line*
819   corresponds to the percentage of the average rainfall produced by the cyclones, at each track point. *Red line* corresponds to the average percentage of 3-hourly rainfall produced by cyclones that is overlapping with lightning impacts. *Green line*, as for lighting, but for rainfall overlapping with diagnosed DC by AMSU. *Magenta line,* as
822   for lightning, but for rainfall overlapping with either lightning impacts or AMSU diagnosed DC. *Blue line*, as for lightning, but for rainfall overlapping with WCBs producing rain. *Grey line* represents the percentage of rainfall that occurs over land areas and does not overlap with either DC or WCBs. **(B)** As in **(A)**, but for the 250 cy-
825   clones producing low rainfall.

828
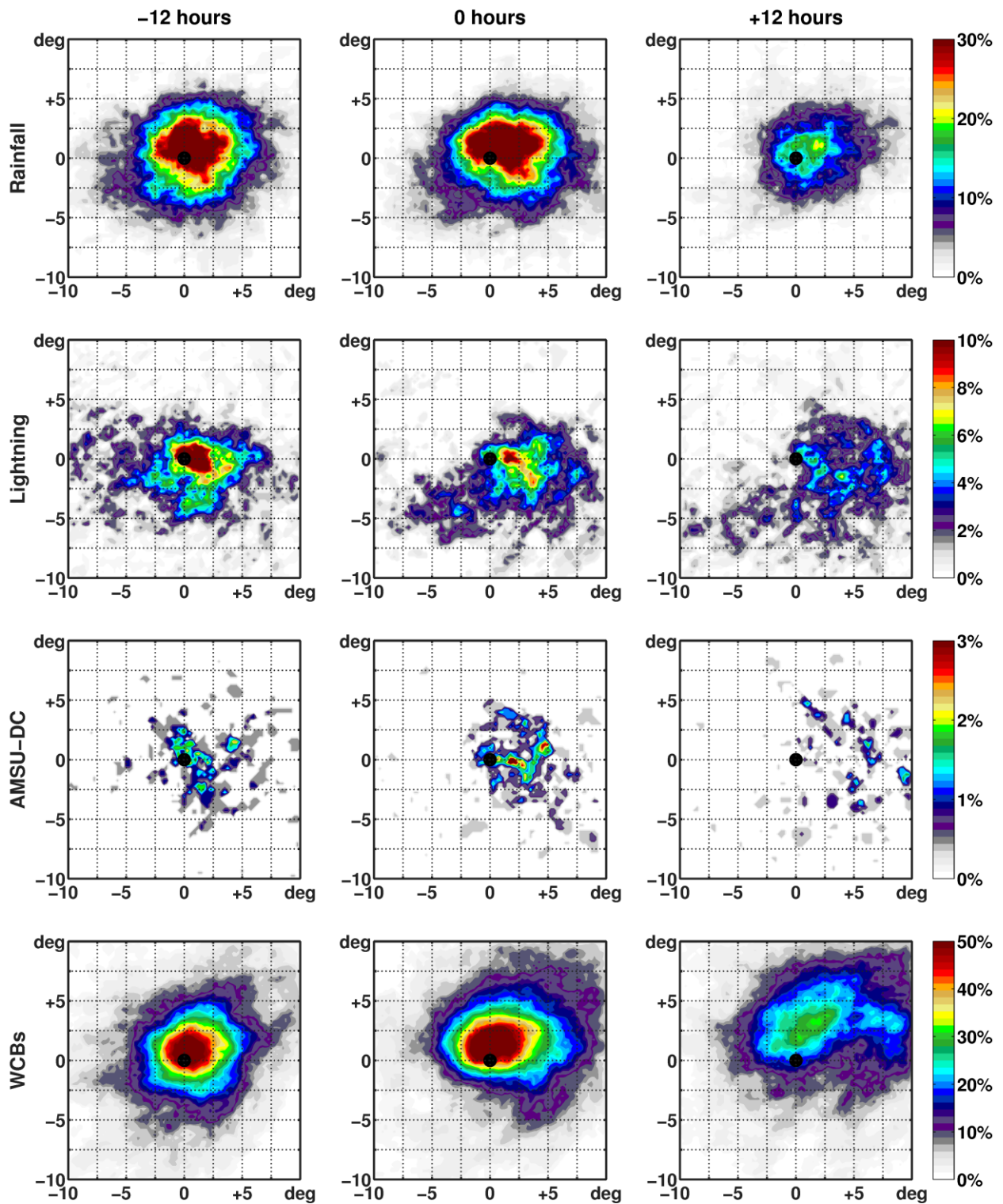
Fig. 7 Probability of occurrence of rainfall, lightning impacts, DC as diagnosed by AMSU and WCBs, with respect to the centre of the 250 cyclones producing high rainfall, at the times −12 h, 0 h and +12 h.

831

834

837

840

843
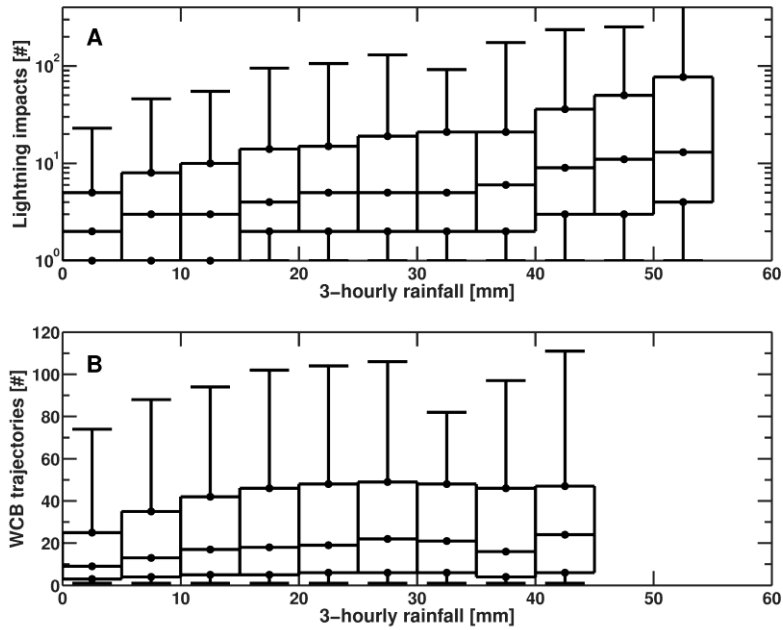
846 **Fig. 8 (A)** Boxplots of number of lightning impacts per bins of 3-hourly accumulated rainfall with a 5 mm width. **(B)** as in **(A)** but for number of WCB trajectories. Note that y-axis in **(A)** is logarithmic. Whiskers denote the 5th and 95th quantile.